Experimental and theoretical study of ultraviolet-induced structural/optical instability in non silicon-based luminescence

Malloy, James; Mantey, Kevin; Maximenko, Yulia; Bahceci, Ersin; Morgan, Huw; Yamani, Zain; Boparai, Jack; Puthalath, Krithik; Nayfeh, Munir H.

Published in:
Journal of Applied Physics

DOI:
10.1063/1.5027307

Publication date:
2018

Citation for published version (APA):
Malloy, J., Mantey, K., Maximenko, Y., Bahceci, E., Morgan, H., Yamani, Z., Boparai, J., Puthalath, K., & Nayfeh, M. H. (2018). Experimental and theoretical study of ultraviolet-induced structural/optical instability in non silicon-based luminescence. *Journal of Applied Physics*, *124*(4), [044501]. https://doi.org/10.1063/1.5027307

Experimental and Theoretical Study of Ultraviolet-Induced Structural/Optical Instability In Nano Silicon-Based Luminescence

James Malloy, Kevin Mantey, Yulia Maximenko, Ersin Bahceci[*], Huw Morgan[**], Zain Yamani[***], Jack Boparai, Krithik Puthalath, and Munir H. Nayfeh

Department of Physics, University of Illinois at Urbana-Champaign, 1110 W. Green Street, Urbana, Illinois 61801, United States of America
[*]Department of Metallurgical and Material Engineering, Iskenderun Technical University, Iskenderun, Turkey
[**] Department of Physics, Aberystwyth University, Penglais, Aberystwyth, Ceredigion, SY23 3BZ, United Kingdom
[***]Department of Physics, King Fahd University, Dhahran 34463, Saudi Arabia

Abstract

Nano silicon is emerging as an active element for UV applications due to quantum confinement-induced widening of the Si bandgap, amenability to integration on Si and less sensitivity to temperature. NanoSi-based UV applications include deep space exploration; high temperature propulsion; solar photovoltaics; and particle detection in high energy accelerators. However, the viability of the technology is limited by a complex nanoSi optical quenching instability. Here, we examined the time dynamics of UV-induced luminescence of sub 3-nm nanoSi. The results show that luminescence initially quenches, but it develops a stability at ~ 50% level with a time characteristic of minutes. Upon isolation, partial luminescence recovery/reversibility occurs with time characteristics of hours. To discern the origin of the instability, we perform first principle atomistic calculations of the molecular / electronic structure in 1-nm Si particles as a function of Si structural bond expansion, using time dependent density functional theory (TD-DFT), with structural relaxation applied in both ground and excited states. For certain bond expansion/relaxation, the results show that the low-lying triplet state dips below the singlet ground state, providing a plausible long-lasting optical trap that may account for luminescence quenching as well as bond cleavage and irreversibility. Time dynamics of device-operation that accommodates the quenching/recovery time dynamics is suggested as a means to alleviate the instability and allow control of recovery, which promises to make it an effective alternative to UV-enhanced Si or metal-based wide-bandgap sensing technology.

Key words: Silicon, nanoparticle, UV-photosensor, triplet, luminescence, structural, instability, reversible, TD-DFT, simulation

Introduction

UV technology utilizes UV-enhanced Si or metal-based wide-bandgap materials (ZnO, MgZnO, III–V materials, Schottky-type TiO), both classes are limited due to lack of blindness to visible light, and non-integralability on Si respectively. The UV-enhanced Si technology is well-established in UV detection and sensing [1], however it still presents some limitations due to the low bandgap energy of Si (1.1 eV), which necessities the use of costly high pass optical filters and phosphors to reject the more abundant low energy photons. Moreover, device performance degrades with temperature, resulting in lower efficiency and higher dark currents. Focus is shifting towards the development of wide-bandgap-semiconductor UV photodetectors, such as those that use GaN-based, diamond, or SiC-based active elements, which eliminate filters and sensitivity to temperature, enabling high-temperature applications [2-6]; however those wide-bandgap material do not integrate on silicon.

One-dimensional (1D) nano structured (i.e., nano wires) UV detectors are attracting attention due to improved sensitivity to light resulting from large surface-to-volume ratio and small Debye length [7]. Enhanced photosensitivity has been observed in ZnO nanowires, Ga_2O_3 nano wires and nano belts, GaN nano wires, and other metal-oxide nano structures [8-11]. However, high-temperature UV detection is still limited due to surface dominated photocurrent transport.

Zero-dimensional (0-D) silicon-based nano structures (nanoparticles) [12-15] are also being considered for UV applications due to large widening of the Si bandgap, and strong enhancement of radiative processes (i.e., highly-luminescent), both induced by quantum confinement, as well as the fact that nanoSi-based material can integrate on silicon. In fact, nanoSi is promising new generation of highly sensitive emitters, optical interconnects, fluorescent tags, markers, sensors or detectors for use in a number of UV intensive environments. UV intensive

applications include deep space exploration; security, commercial, and consumer applications including military high temperature propulsion (rockets, missiles, fighter jets, and nuclear detonation) [16-21]; solar photovoltaics [22-23] as well as particle detectors in high energy accelerators [24]. Recent measurements however showed that nanoSi-based devices are limited as the material exhibits partial quenching, with time characteristic of minutes to hours depending on the UV intensity, beyond which it develops stability at ~ 50% level [25-26]. Yet nanoSi is still promising in view of the fact that organic dyes under similar conditions get quenched over much shorter time without developing any residual stability. However, to provide viable nanoSi-based devices as well as to achieve their full potential, the stability issue must be understood. In fact, the stability behavior remains in question, both experimentally and theoretically. There are no measurements to discern whether the quenching is permanent or non-permanent and to what degree it is reversible. Moreover it is not known if the instability is of chemical, physical or UV-induced bond-cleavage. Theoretically, there are no studies of structural relaxation in the UV-pumped exited states, whether singlet or triplet states, atomic mechanical strain and UV-induced cleavage of bonds. It is not clear what would the interplay be among the other miniaturization-induced effects, such as breaking of symmetry and degeneracy, singlet-triplet (S-T) splitting, etc.

In this paper we conduct experimental and theoretical studies to shed light on the UV-induced instability of nano silicon-based active elements. We measure the time dynamics of photoluminescence, for single as well as multiple cycles of interactions, during UV-pumping to determine the characteristics of quenching; as well as after isolation from the UV radiation to measure branching ratio of reversible VS non-reversible luminescence. We also examine the behavior under reactive and non-reactive environment to examine the origin of non-reversible luminescence. Theoretically, we calculate the molecular structure and the effect of structural

relaxation in the excited particles utilizing first principle atomistic calculations. The eigenenergy and wavefunction and S-T splitting are calculated for the ground and excited singlet and triplet states as a function of relaxation coordinates, with the excited state calculated at the time dependent density functional theory (TD-DFT) level. Those will be used to identify plausible long-lived traps, as well as to compare prospective pathways for excitation and emission with the experimental results.

I. Experimental

Light induced electrochemical etching of Si in HF was used to generate luminescence from silicon [27-28]. Here we produce ultrasmall luminescent Si nanoparticles by H_2O_2 - induced chemical etching of Si in HF. (001) single-crystal boron-doped silicon wafers with resistivity in the range 4–8 Ω-cm are etched in an HF / H_2O_2 mixture using electrical or hexachloroplatinic acid catalyst [29-34]. After the treatment, the wafers are sonicated in a liquid of choice. The surface of the particles is terminated with hydrogen. Such Si–H bonds are a key to silicon chemistry, enabling a variety of chemical routes for attachment with hydrocarbons and biomedically important molecules. The nanoparticles stay in suspension for easy recovery and reuse. The chemical procedure predominantly produces red luminescent particles of dominant size of 2.9 nm in diameter. **Figure 1a** gives TEM image of a typical nanoparticle sample deposited on graphite grid; a histogram gives counts of 4, 56, 12, 9, and 2 at diameters of 3.5, 2.9, 2.2, 1.7, and 1 nm. To obtain the luminescence spectra, we excite particle colloids by 365-, 300- or 254-nm incoherent light. For detection, we use a fiber optic spectrometer, equipped with optical fibers to extract the emission and a holographic grating. It is a near-infrared grating with groove density of 600/mm with a blaze wavelength of 0.4 μm and with best efficiency in the range 0.25–0.80 μm. The luminescence spectrum of a colloid with a peak at 2.9-nm Si nanoparticles dispersed in isopropanol

alcohol under UV-excitation at 300 nm is a wide band over the range 550–750 nm with a band maximum at 620 nm as shown in **Figure 1b**. Unlike direct-bandgap nanoparticles, which emit sharp lines, indirect-bandgap nanoparticles emit broad bands due to structural relaxation [35-40].

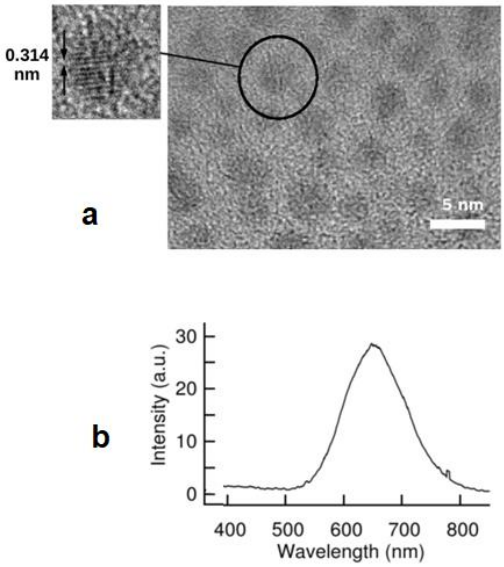

Figure 1

In the electric method and when the current is high, the etching rate is high and nanoparticles are produced with smaller average size. **Figure 2a** gives a TEM image of a typical sample with a dominant particle size of 1-nm. **Figure 2b** gives the luminescence spectrum of such distribution in solution using 365-nm excitation. Quantum Monte Carlo (QMC) calculations of 1-nm Si nanoparticle employing Hartree-Fock pseudopotentials confirm reconstruction in which there is stripping of some hydrogen by H_2O_2 and movement of surface Si atoms (1.5Å each) from the next-nearest spacing of 5.4 Å to the tetrahedral 2.36-Å spacing, to form novel dimer surface phase [41-43] (**Figure 2c,** right**)**.

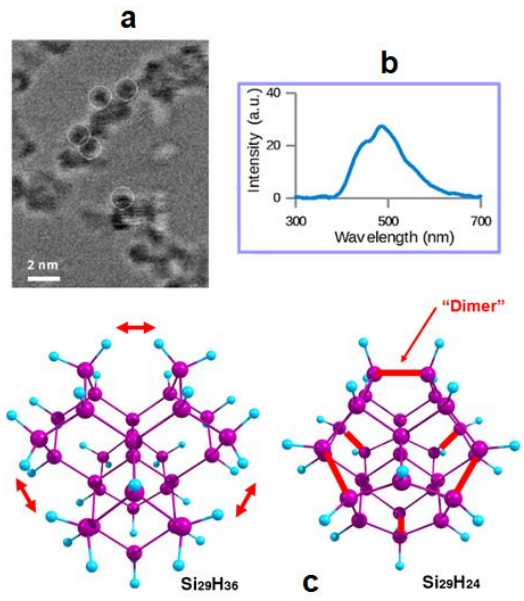

Figure 2

We use two samples of different average size of nanoparticles, 2.9-nm and 1-nm, having confinement bandgap energies of 2.1 and 3.5 eV respectively; and we use UV radiation at photon energy 3.5 eV, and 5.4 eV (wavelengths 365 nm and 254 nm) for excitation. Thin solid films for measurements are prepared by drop-drying on device-quality silicon. Scanning electron microscope (SEM) shows different degrees of packing. Nanoparticle ensembles are illuminated in near-grazing incidence by UV radiation, while a fiber optic monitors the luminescence in the perpendicular direction through UV filters. Samples are placed in thermal contact with large substrates to limit temperature rise to few degrees. The photoluminescence is obtained by using dispersive holographic gratings. We excite with incoherent CW UV radiation with intensities of ~ 10^{14} photons /cm^2. While being under illumination, the luminescence spectra were recorded at several times. The sample is then isolated from UV and the luminescence is recorded at several times by very brief exposures to UV to avoid additional quenching. We also tested suspensions of

silicon nanoparticles in liquid, which are prepared by placing 0.35 ml of the colloid samples into narrow quartz cuvettes.

II. Results

Figure 3a displays the peak intensity of the luminescence with time for the ~ 2.9-nm particle-film. It present data during the continuous exposure period, displaying luminescence quenching from an initial arbitrary count of 37.5 and developing a plateau at a count of 19 or nearly 50 percent level. After reaching the stability plateau, UV irradiation is discontinued and the sample is left isolated. Luminescence is then measured with time using very brief exposure to UV. **Figure 3b** displays the results; it shows luminescence recovery but only to a count of 31.5 or 80 percent of the original intensity, i.e., the luminescence has 20 percent irreversibility. Analysis shows a recovery time constant ~ 20 ± 0.5 hours. Different particle coverage showed insignificant changes, indicating particle networks are not responsible for the long time scale. Analyzing the time dynamics using the integrated band intensity showed insignificant differences from the results using the peak intensity. After recovery, the sample was subjected to a second cycle of quenching/recovery. The result for two cycles are shown in **Figure 3c**. It shows the intensity recovers to 25.4 from an initial 31.5 or 80 percent recovery for the second cycle, indicating again an irreversibility of 20 percent.

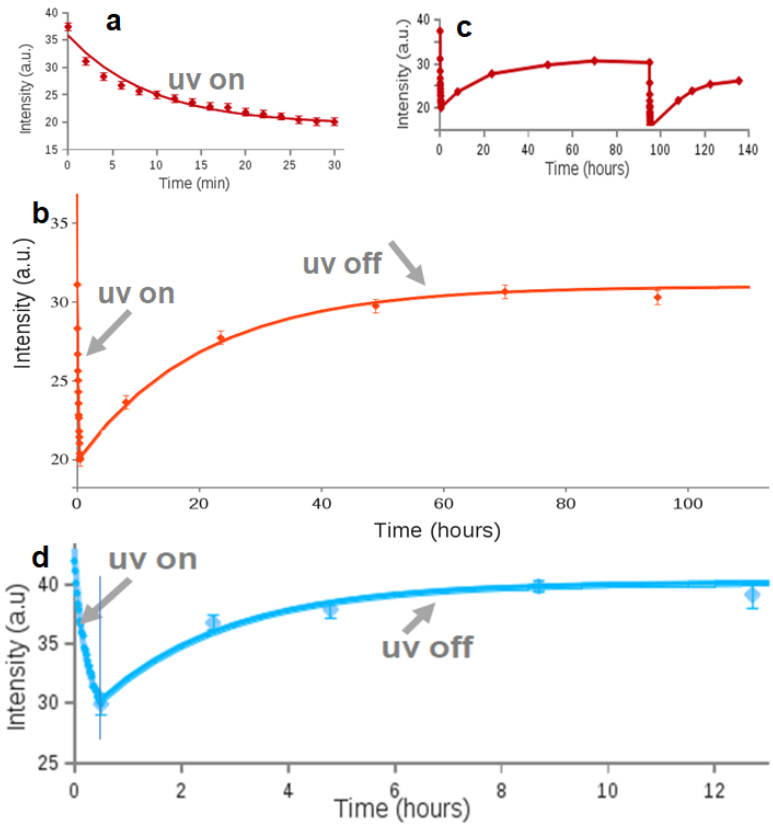

Figure 3

Figure 3d presents measurements of 1-nm particles (3.29-eV bandgap) (taken in solution) using 365-nm excitation (spectrum in **Fig. 2b)**. The measurements give recovery times of 19.5 ±0.5 hours, which is comparable to the recovery time obtained for the 2.9-nm particle (~ 20 ± 0.5 hours). We also compared results for exciting films of 2.9-nm particles with 365-nm and with 254-nm radiation photons. The results (not shown) show 365-nm excitation (< twice the bandgap) displayed similar recovery times to those using 254-nm excitation (> twice the bandgap), indicating insignificant multi-exciton effects. Moreover, those results show that the irreversibility for the 2.9-nm particle is the same as that for the 1.0-nm particle.

The irreversibility could be due to change in the chemical composition, H-passivation, restructuring or disintegration. The 2.9-nm film was continuously exposed at room-temperature

under flow of N_2/Ar gas. No significant differences are found for measurements taken under ambient conditions. **Figure 4** presents selected spectra during the continuous exposure, and during the recovery, showing essentially similar spectra, which suggests that the UV treatment did not change the composition or cause disintegration of the core of all the particles in the sample since the spectral distribution of emission depends on particle size.

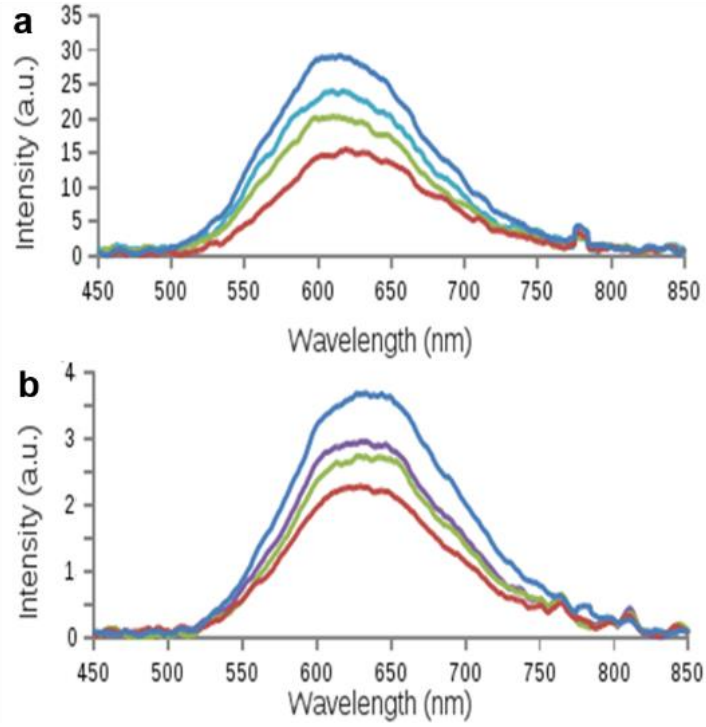

Figure 4

III. Theory and Simulation

We use first principle atomistic calculations to calculate the molecular structure of 1-nm silicon nanoparticles as a model system to identify long-lived traps. 2.9-nm particles are not amenable to such simulations but 1-nm particles are small enough to carry out such simulations. We use the restructured 1-nm particle ($Si_{29}H_{24}$ with 6 reconstructed dimers (**Fig 2c**). The excited

state was calculated at the time dependent density functional theory (TD-DFT) level using the B3LYP functional with the TURBO-MOLE quantum computational package [44-46].

The TZVP basis was used which is a triple split valence basis with polarization functions added for each atom. In the simulation, a dimer bond is stretched; then the nuclei are relaxed to minimize energy. Because nano particles are expected to become less elastic when they are excited, and hence they would relax differently upon excitation, we must perform the relaxation step both before excitation (i.e. in the ground state), as well as after excitation (i.e. in the excited state) when determining pathways for absorption/emission.

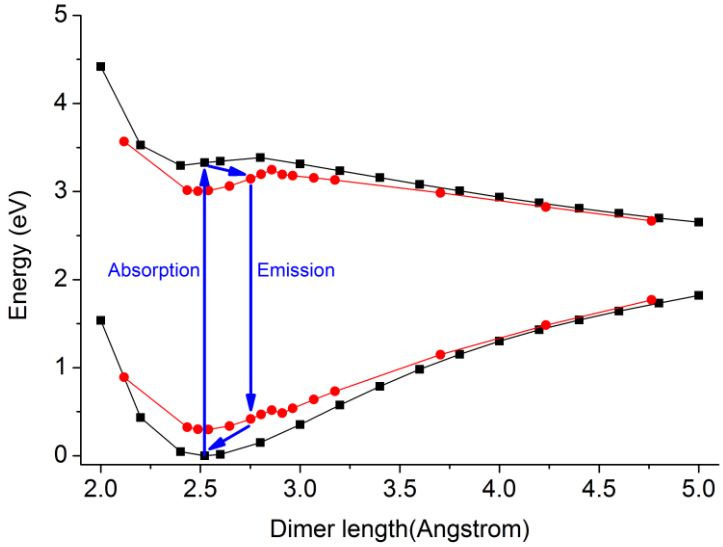

Figure 5

Figure 5 presents an energy level diagram of the particle, consisting of only the ground and first excited singlet state [46]. All energies are relative to the ground state minimum. The energy of this excited state defines the bandgap of the particle. The ground state, which is highest occupied molecular orbital (HOMO) is calculated twice: before absorption, i.e., before the particle is excited and when the particle is excited. In those two states the position of the nuclei are different and transition between the states occurs by simple relaxation of the nuclei. The first excited state

is similarly calculated twice: before the particle is excited and when the particle is actually excited. The structures were calculated with one dimer stretched and constrained to a given length *R* and the structure having C2v symmetry. The figure shows several features. First, the potential curves for both the ground and excited states exhibit a well with a minimum at R = 2.36 Å, the tetrahedral reaction coordinate, a barrier at an extended reaction coordinate of $R \sim 3$ Å, and a dissociation limit at ~ 5.4 Å. Second, relaxation in the excited state decreases the inner well excited state by 0.28 eV, and also increases the ground state inner well by 0.30 eV. Third, in the outer region (beyond the barrier) the energies obtained using optimization in the ground state and excited state converge. The figure shows an example of a pathway cycle for absorption/relaxation/emission/relaxation. Absorption is a vertical excitation process from the ground state energy minimum (optimized before absorption) to the excited state (of that same geometry (optimized before absorption). The structure can then change (relax) to one of lower energy in the excited state (optimized after absorption), where emission occurs to the ground state of this new structure (ground state optimized after absorption), then will relax back to the initial state (ground state optimized before absorption). The emitted photon energy is therefore overestimated by 0.58 eV if the particle is not optimized in the excited state.

The minimum excitation energy is 3.29 eV as can be also seen in **Figure 5**. This is associated with the bandgap of the particle. The barrier height between the inner and outer region is now 3.25 eV (relative to the minimum ground state structure). As the minimum excitation energy is 3.29 eV, this means direct excitation over the barrier is energetically allowed. Beyond the barrier in the outer region the ground state optimized and excited state optimized energies converge, showing that the ground state optimized geometry is a good approximation for the excited state optimized geometry in the outer region. In the entire inner well and at the barrier the energy

difference between the excited state and ground state remains close to 2.7 eV. Emission at the barrier would be 2.73 eV (455 nm).

We calculate in a similar way the minimum excitation of other excited states. We focus on the valley states, namely lowest unoccupied molecular orbital (LUMO) manifold at the minimum of the electron conduction band. **Figure 6** presents the results; there are three valley states. The lowest energy state, an *A*1-state, is completely non-degenerate; the second lowest state, an *E*-state, is doubly-degenerate; and the highest in the manifold, a *T*2-state, is triply-degenerate. The energy of the three states are 3.29, 3.5, and 3.55 eV respectively. This manifold corresponds to the six-fold degenerate in bulk lowest manifold. In the particle, it splits into only three energy states. The lowest *A*1-state (whose potential surface was shown in detail in **Figure 5** defines the bandgap at 3.29 eV. The next state (*E*-state) in this valley is 210-meV above the *A*1-state, which is much larger than the thermal agitation energy kT. It is known that in ultrasmall nanoparticles, where translational symmetry is significantly broken such multiplicity [47] arises and valley splitting correlates with size reduction [48].

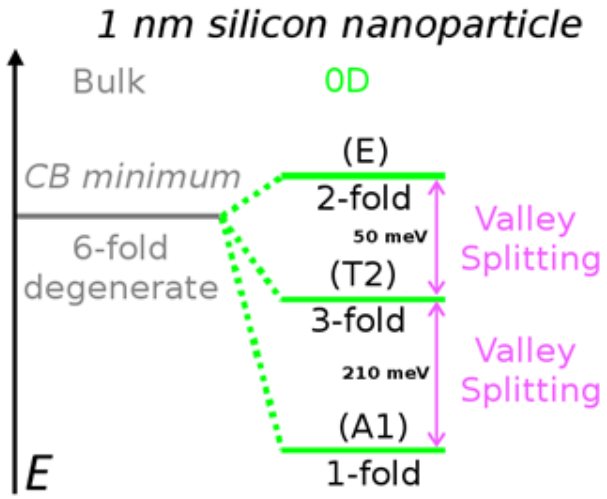

Figure 6

It has been suggested that the Si-Si dimers are excitonic self-traps on which radiative recombination, hence luminescence takes place [36-37]. Thus we now calculate the lowest triplet state on a Si-Si dimer, which may serve as trap state for electron excitation. To discern its nature, we calculate the ground, first singlet (S), and first triplet (T) excitonic states, and deduced the S-T splitting as a function of the Si-Si bond length. To simplify the simulation, we use a 1-nm particle with a single dimer reconstruction, namely $Si_{29}H_{34}$. For this configuration, the minimum at R = 2.36-Å dimer length of lowest non-degenerate valley state, (see **Figure 6,** the singlet $A1$ state (the lowest of the $B2$ irreducible representation) lies at 4.4 eV instead of 3.29 eV (the bandgap). The states, shown in **Figure 7**, were optimized individually using TD-DFT along the reaction coordinate of the dimer bond R. Within the inner region, the splitting is complicated. Beyond the barrier, it is boosted to 1.7 eV. Large splitting (120-meV splitting) was previously shown in 1-nm nanowires with [49]. Now for stretched dimer (> 4.3 Å), the triplet state dips below the singlet ground state; becoming the ground state with a 2.85-eV minimum. Stretching to 5.4 Å dissociates or break the bond, where excitons may combine nonradiatively. Non-radiative recombination sites results in a permanent loss (irreversible) luminescence. Also it was previously noted that triplets in unconstructed $Si_{29}H_{36}$ may dip below the ground state upon expanding a Si-Si bond and may break it [50]. We show in **Figure 7** some pathways for excitation to higher triplets followed by inverse internal conversion to the singlet ground state. These processes are akin to limiting processes in photosynthesis molecules [51].

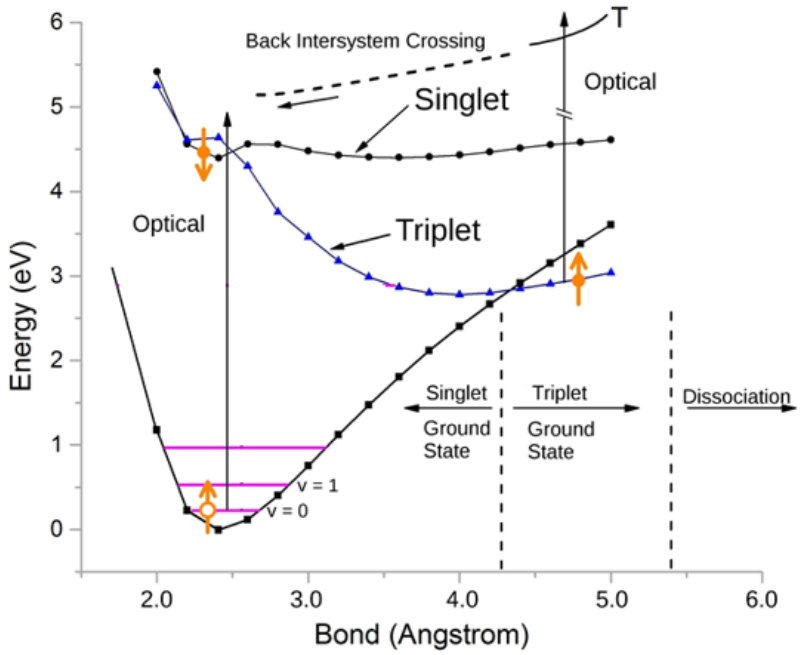

Figure 7

We demonstrate trapping on dimers by calculating the charge distribution within the particle. We display the electron-hole wavefunctions using the MacMolPlt visualization program [52]. The molecular orbitals for $Si_{29}H_{24}$ are depicted using wavefunction density isosurfaces. **Figure 8a** shows the charge distribution for a dimer bond (reaction coordinate) of 2.4 Å (un-stretched dimer, at bottom of inner-well). The HOMO (singlet hole ground state), given on the left and the LUMO (singlet electron excited state), given on the right of the figure show that the orbitals are de-localized throughout the nanoparticle. At separations larger than 2.8 Å the orbital density for the HOMO and LUMO become strongly concentrated on the stretched dimer. For example for a dimer stretched to 3 Å, shown in **Figure 8b**, the HOMO (on the left) and LUMO (on the right) in the outer region strongly resemble the bonding and antibonding of a dimer isolated from the rest of the nanoparticle. When confined on the same dimer, the electron and hole's wavefunctions overlap; increasing the exchange integral and the S-T splitting significantly. The giant S-T splitting

is due to a dramatic localization (trapping) of the electron and hole, being in the same place at the same time.

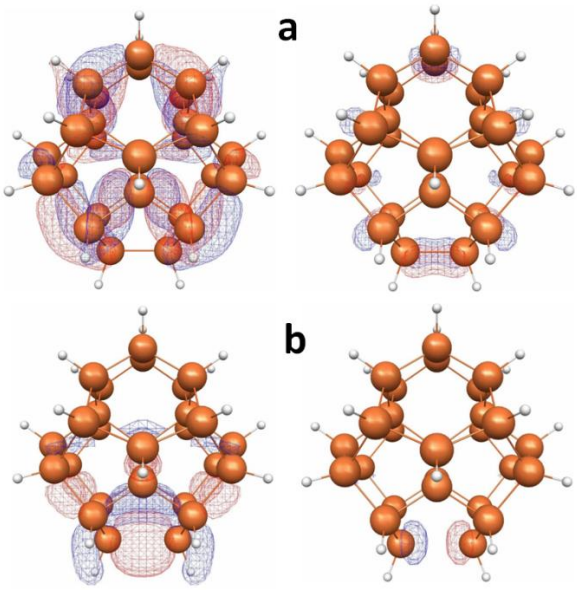

Figure 8

IV. Discussion

Figure 7 presented some excitation/emission pathways. A plausible process involves a process in which UV irradiation excites an electron "vertically", followed by nuclear rearrangement/relaxation and dimer stretch. Intersystem crossing occurs causing a spin flip. With dimer stretching, the electron and hole get trapped on the bond (**Figure 8)** lowering the triplet state energy. The triplet becomes populated and emission is no longer available, indicating long lifetime as measured. Reversed crossing from the stretched triplet to the stretched ground singlet, followed by relaxation to the bottom of the singlet well re-opens luminescence.

Figures 3 show that a fraction of the excited particles may suffer Si-Si cleavage**.** Upon self-trapping of a photo-excited electron-hole pair on a reconstructed Si-Si bond, there is some

probability that it may expand enough to reach a bond length of 5.4 A, namely reversing the reconstruction, which removes it as a radiating site.

Since quenching takes place on a scale of minutes while the recovery time occurs on the scale of hours, the stability of the device can be improved by operating in a pulsed mode with a low duty cycle to allow ample time for the sensor to recover. From **Figures 3**, it is best to set the ratio of time between pulses (off) to the pulse duration (on) off/on > 60, or with a duty cycle of < 1/60. Excitation using microsecond pulsed beams at rates 10-10^4 Hz fall in this range. In fact, pulse mode test measurements of luminescence quenching were taken using yttrium aluminum garnet (Nd:YAG) laser irradiation at a wavelength of 355 nm, with10 ns per pulse at 10 pulses per second [25]. Despite the fact that the average radiation power at the target is 20 mW/cm^2 (~ 2-orders of magnitude higher than what is used in the present CW measurement), the quenching time scale was as long as 5 hours (~ an order of magnitude longer than in the CW case). Excitation using picosecond or nanosecond pulsed systems can easily satisfy this condition. For two photon excitation, a mode locked femtosecond Ti-sapphire near infrared laser system, generating pulses of 150 fs duration in the wavelength range of 750-840 nm at a repetition rate of 80 MHz can also be useful in this regard.

V. Conclusion

In conclusion, we examined the viability of sub 3-nm nano-silicon-based uv photosensors. We showed that the luminescence under intense UV radiation gets quenched before developing a long-term stability at ~ 50% level, with near 80 percent reversibility upon isolation from the radiation with a long-time scale of hours. This is unlike organic dyes which do not develop any level of stability under UV irradiation. First principle atomistic calculations of the molecular /

electronic structure of 1-nm Si particles using time dependent density functional theory (TD-DFT) identified a novel singlet-triplet (S-T) intercrossing in which the triplet state dips below the singlet state, providing a long-lasting optical trap. Time dynamics of device-operation that accommodates the quenching/recovery time dynamics is suggested as a means to alleviate the instability and allow control of recovery, hence render nano silicon as an effective alternative to UV-enhanced Si or metal-based wide-bandgap sensing technology.

References

1. C. M. Pepin, H. Dautet, and M. Bergeron et al., in Proc. 2010 Nucl. Sci. Symp. Conf. Rec., 1740 (2010).
2. T. Toda, M., Hata, Y. Nomura, Y. Ueda, M. Sawada, M. Shono, Jpn. J. Appl. Phys, *43*, L27 (2004).
3. M.Y. Liao, Y. Koide, J. Alvarez, Appl. Phys. Lett., *87*, 022105:1 (2005).
4. E. Munoz, Phys. Stat. Sol. *(b)*, *244*, 2859 (2007).
5. L.W. Sang, M.Y. Liao, Y. Koide, M. Sumiya, Appl. Phys. Lett., *99*, 031115:1 (2011).
6. L.W. Sang, M.Y. Liao, Y. and M. Sumiya, Sensors, 13, 10482 (2013).
7. T.Y. Zhai, X.S. Fang, M.Y. Liao, X.J. Xu, H.B. Zeng, Y. Bando, D.A. Golberg, Sensors, 9, 6504 (2009).
8. K. Keem, H. Kim, G.T. Kim, J.S. Lee, B. Min, K. Cho, M.Y. Sung, S. Kim, Appl. Phys. Lett., 84, 4376 (2004).
9. C. Soci, A. Zhang, B. Xiang, S.A. Dayeh, D.P.R. Aplin, J., Park, X.Y., Bao, Y. H., Lo, D., Wang, Nano Lett., 7, 1003 (2007).
10. Q. Yang, X. Guo, W. Wang, Y. Zhang, S. Xu, D.H. Lien, Z. L. Wang, ACS Nano, 4, 6285 (2010).
11. X. S. Fang, Y. Bando, M.Y. Liao, U. K. Gautam, C.Y. Zhi, B. Dierre, B. D. Liu, T. Y. Zhai, T. Sekiguchi, Y. Koide, *et al*. Adv. Mater., 21, 2034 (2009).
12. M.I Baratron, ed., *Synthesis, Functionalization, and Surface Treatment of Nanoparticles* American Scientific Publishers, (2002).
13. V. Kumar, ed., *Nanosilicon*, Elsevir, (2007).
14. M. H. Nayfeh, *Fundamentals and applications of nano silicon in plasmonics and fullerenes: current and future trends* Elsevier Publishing, (2018)

15. L. Pavesi, S. Gaponenke, and L. D. Negro, eds., *Towards the first silicon laser*, Kluwer Academic Publishers, (2003)

16. O. Nayfeh, S. Rao, A. Smith, J. Therrien, and M. Nayfeh, Photonic Technology Letters, 16, 1927 (2004).

17. M. Nayfeh, S. Rao, O. Nayfeh, A. Smith, J. Therrien, IEEE Transcations on Nanotechnology, 4, 660 (2005).

18. M. Krause, M. Topic, H. Stiebig, and H. Wagner, Phys. Stat. Sol A, 185, 121 (2001).

19. J. M. Pimbley and G. J. Michon, IEEE Trans. Electron Devices, ED-34/2, 294 (1987).

20, D. Berman, M. Aceves, L. R. Berriel et. al., Phys. Stat. Sol. (c), 1, 1 (2004).

21. D. M. Brown, E. T. Downey, M. Ghezzo, J. W. Kretchmer, R. J. Saia, Y. S. Liu, J. A. Edmond, G. Gati, J. M. Pimbley, and W. E. Schneider, IEEE Trans. Electron Devices, 40, 325 (1993).

22. M. Stupca, M. Alsalhi, T. Al Saud, A. Almuhanna, and M. H. Nayfeh, Appl. Phys. Lett. 91, 063107 (2007).

23. F. I. Chowdhury, M. Nayfeh, and A. Nayfeh, The Journal of Solar Energy 125, 332 (2016).

24. S. Magill, J. Xie, M. Nayfeh, H. Yu, M. Fizari, J. Malloy, Y. Maximenko, J of Instrumentation 10, 05008 (2015).

25. M. Nayfeh, A. Kumar, L. D. Stephenson, and A. J. Nelson, K. Mantey, M. Kwit, J. Appl. Phys. 107, 064316 (2010).

26. O. M. Nayfeh, T. Hoang, and M. H. Nayfeh, B. Alhreish and J. Boparai, A. AlDwayyan and M. AlSalhi, J. Appl. Phys. 112, 074313 (2012).

27. L. T. Canham., Applied Physics Letters, 57, 1046 (1990).

28. M. J. Sailor, *Porous Silicon in Practice: Preparation, Characterization and Applications,* Wiley-VCH, Weinheim, (2011).

29. O. Ackakir, J. Therrien, G. Belomoin, N. Barry, J. Muller, E. Gratton, and M. Nayfeh, Appl. Phys. Lett. 76, 1857 (2000).

30. G. Belomoin, J. Therrien, A. Smith, S. Rao, R. Twesten, S. Chaieb, M. H. Nayfeh, L. Wagner, and L. Mitas, Appl. Phys. Lett., 80, 841 (2002).

31. L. Mitas, J. Therrien, R. Twesten, G. Belomoin, and M. H. Nayfeh, Appl. Phys. Lett., 78, 1918 (2001).

32. D. Nielsen, L. AbuHassan, M. Alchihabi, A. Al-Muhanna, J. Host, and M. H. Nayfeh, J. Appl. Phys 101, 114302 (2007).

33. M. H. Nayfeh and L. Mitas, V. Kumar, ed. Elsevir, 1 (2007).

34. M. Nayfeh, M. Alamri, M. M. El Gomati, and M. S. Zubairy, Springer (2016).

35. G. Allan, C. Delerue, M. Lannoo and E. Martin, Phys. Rev. B, 52, 11982 (1995).

36. G. Allan, C. Delerue and M. Lannoo, Phys. Rev. Lett., 76, 2961 (1996).

37.M. Nayfeh, N. Rigakis, and Z. Yamani, Phys. Rev. B, 56, 2079 (1997).

38.M. Cazzanelli, D. Navarro-Urriós, F. Riboli, N. Daldosso, L. Pavesi, J. Heitmann, L.X. Yi, R. Scholz, M. Zacharias and U. Gösele Journal of Applied Physics, 96, 3164 (2004).

39. L.W. Wang and A. Zunger, J. Phys. Chem., 98, 2158 (1994).

40. L. Mitas, J. Therrien, R. Twesten, G. Belomoin, and M. H. Nayfeh, Appl. Phys. Lett., 78, 1918 (2001).

41. Z. Yamani, H. Thompson, L. AbuHassan, and M. H. Nayfeh, Appl. Phys. Lett., 70, 3404 (1997).

42. L. Wagner, A. Puzder, A. Williamson, Z. Helms, J. C. Grossman, L. Mitas, G. Galli, and M. Nayfeh, arXiv, 1 (2004).

43. G. Belomoin, E. Rogozhina, J. Therrien, P. V. Braun, L. Abuhassan, M. H. Nayfeh, L. Wagner, and L. Mitas, Phys. Rev. B, 65, 193406 (2002).

44. M. H. Nayfeh and L. Mitas, in *Nanosilicon*, V. Kumar, ed. Elsevir, 1 (2007).

45. S. Rao, J. Sutin, R. Clegg, E. Gratton, S. Habbal, M. H. Nayfeh, A. Tsolakidis, and R. Martin, Phys. Rev B, 69, 205319 (2004).

46. K. A. Mantey, *Structure, electronic levels, and ionic interactions of 1 nm silicon particles https://www.ideals.illinois.edu/bitstream/handle/2142/26172/Mantey_Kevin.pdf?...1*by KA Mantey, University of Illinois at Urbana-Champaign (2011)

47. M. P. Persson and H. Q. Xu, Physica Scripta, T101, 147 (2002).

48. K. Leung and K. Whaley, Phys. Rev B, 56, 7455 (1997).

49. M. Palummo, F. Iori, R. Del Sole, and S. Ossicini, Phys. Rev. B, 81, 121303 (2010).

50. O. Lehtonen and D. Sundholm, Phys. Rev B, 72, 085424 (2005).

51. A. Jabłoński, Nature, 131, 839 (1933).

52. B. M. Bode and M. S. Gordon, J. Mol., Graphics and Modeling, 16, 133 (1998).

Figure Captions

Figure 1 (a) high resolution transmission electron microscope (HRTEM) image of silicon nanoparticles with a dominant diameter of 2.9-nm placed on a graphite grid from a colloid sample. The zoom-in of a particle showing the silicon atomic planes (b) luminescence spectrum of the precursor colloid sample using excitation at 365 nm wavelength.

Figure 2 (a) TEM of silicon nanoparticle with a dominant diameter of 1-nm placed on a graphite grid (b) The luminescence spectrum of the precursor colloid sample using 365-nm excitation. (c) Molecular configuration of 1 nm silicon nanoparticle (left) bulk-like ($Si_{29}H_{36}$) and (right) the fully restructured 1 nm silicon nanoparticle ($Si_{29}H_{24}$). Silicon atoms are purple and hydrogen atoms are light blue.

Figure 3 Time dynamics of the peak of the luminescence band of 2.9-nm nanoparticles under UV treatment (a) taken during continuous exposure to UV radiation showing quenching and stability plateau (b) taken after turning off the UV irradiation (UV exposure discontinued) showing some recovery. The plot also shows the early period of quenching thus it constitute a full cycle of quenching/recovery (c) two cycles of quenching/recovery. (d) Measurements of quenching and recovering of photoluminescence for a sample dominated by 1 nm Si nanoparticles.

Figure 4 Selected luminescence bands of a film sample dominated by 2.9-nm nanoparticles (a) during irradiation and (b) during recovery.

Figure 5 Schematic energy level diagram near the minimum of the conduction band of a fully reconstructed 1-nm nanoparticle ($Si_{29}H_{24}$).

Figure 6 The ground and excited state energies as a function of the reaction coordinate *R* (a dimer bond length) calculated with structures relaxed in the ground state (black, squares), along with the ground and excited state energies with structures relaxed in the excited state (red, dots). All energies are relative to the ground state minimum (at R = 2.36 Å). The structures were calculated with one dimer stretched, constrained to a given length, and the structure having C2v symmetry. Absorption (excitation) proceeds vertically up from the ground state minimum to the excited state followed by relaxation; and the emission proceeds vertically down from the excited state to the ground state, followed by relaxation back to the ground state minimum.

Figure 7 The calculated ground state, first excited singlet and first triplet state in a 1-nm silicon nanoparticle ($Si_{29}H_{34}$) are plotted as a function of the bond length of a single restructured Si-Si molecule-like dimer *R*. UV absorption (excitation) proceeds vertically up from the ground state minimum, followed by intersystem crossing to the triplet state.

Figure 8 Distribution of molecular orbital density in 1-nm Si nanoparticles ($Si_{29}H_{24}$). (a) (left) HOMO and (right) LUMO for an unstretched dimer length of 2.4 Å (Td symmetry). (b) (left) HOMO and (right) LUMO for a stretched dimer length of 3 Å (Cs symmetry). The isosurface shown has the value 25% $(\Psi_{max})^2$ for the diffuse HOMO and 50% $(\Psi_{max})^2$ for the LUMO

.